



# Advancements in the fabrication and characterization of actinide targets for superheavy element production

Ch. E. Düllmann<sup>1,2,3</sup> · E. Artes<sup>1,2,3</sup> · A. Dragoun<sup>1,3</sup> · R. Haas<sup>1,2,3</sup> · E. Jäger<sup>2</sup> · B. Kindler<sup>2</sup> · B. Lommel<sup>2</sup> · K.-M. Mangold<sup>4</sup> · C.-C. Meyer<sup>1,3</sup> · C. Mokry<sup>1,3</sup> · F. Munnik<sup>5</sup> · M. Rapps<sup>1,3</sup> · D. Renisch<sup>1,3</sup> · J. Runke<sup>1,2</sup> · A. Seibert<sup>6</sup> · M. Stöckl<sup>4</sup> · P. Thörle-Pospiech<sup>1,3</sup> · C. Trautmann<sup>2,7</sup> · N. Trautmann<sup>1</sup> · A. Yakushev<sup>2</sup>

Received: 24 June 2022 / Accepted: 14 October 2022 / Published online: 24 November 2022  
© The Author(s) 2022

## Abstract

The heaviest elements can exclusively be produced in actinide-target based nuclear fusion reactions with intense heavy-ion beams. Ever more powerful accelerators deliver beams of continuously increasing intensity, which brings targets of current technology to their limits and beyond. We motivate efforts to produce targets with improved properties, which calls for a better understanding of targets produced by molecular plating, the current standard method. Complementary analytical methods will help shedding more light on their chemical and physical changes in the beam. Special emphasis is devoted to the aspect of the optimum target thickness and the choice of the backing material.

**Keywords** Superheavy elements · Actinide targets · Heavy-ion beam · Target backing · Molecular plating · Thin film analytics

## Introduction

The heaviest known elements are produced in heavy-ion fusion reactions using beams at Coulomb barrier energies [1, 2]. The beam passes a backing and then enters a target, where it induces complete fusion leading to a compound nucleus that contains all nucleons of the projectile and the target nuclei; fusion products recoil from the point of

creation within the target with the momentum of the beam. Depending on the minimum excitation energy,  $E^*$  (or: temperature) at which compound nuclei can be produced, the reactions are referred to as either “cold fusion” or “hot fusion”. Cold fusion reactions are based on targets of  $^{208}\text{Pb}$  or neighboring nuclei, stabilized by shell closures at atomic number  $Z=82$  and/or neutron number  $N=126$ . These targets are irradiated by medium heavy projectiles leading to elements up to Cn (element 112) [3] and Nh (element 113) [4]. Hot fusion reactions, employed for elements up to Og (element 118) [1] are based on actinide targets, irradiated with lighter projectiles.

Cold-fusion reactions typically lead to more neutron-deficient isotopes than hot-fusion ones. The heaviest elements accessible with cross sections of at least 100 fb are Cn for cold fusion reactions, whereas this limit is reached only at Og in actinide-target based reactions. Therefore, all elements with  $Z \geq 114$  are only accessible in the latter reaction type. The mechanical target stability becomes a pressing issue in superheavy element (SHE) research [5, 6], not least due to upgrades [7] and R&D activities [8] and construction of altogether new accelerators [9, 10] that will provide ever more intense beams. Therefore, the production of high-quality targets that withstand intense heavy ion beam bombardment for extended periods is of prime importance.

Presented at the 19th Radiochemical Conference (RadChem 2022) held in Mariánské Lázně, Czech Republic, on 15–20 May 2022.

M. Rapps — Deceased

✉ Ch. E. Düllmann  
duellmann@uni-mainz.de

- <sup>1</sup> Johannes Gutenberg University Mainz, Mainz, Germany
- <sup>2</sup> GSI Helmholtzzentrum für Schwerionenforschung GmbH, Darmstadt, Germany
- <sup>3</sup> Helmholtz Institute Mainz, Mainz, Germany
- <sup>4</sup> DECHEMA-Forschungsinstitut, Frankfurt, Germany
- <sup>5</sup> Helmholtz-Zentrum Dresden-Rossendorf, Dresden, Germany
- <sup>6</sup> European Commission, Joint Research Center (JRC), Karlsruhe, Eggenstein-Leopoldshafen, Germany
- <sup>7</sup> Technische Universität Darmstadt, Darmstadt, Germany

Excitation functions governing the production of heaviest nuclei differ in a many aspects between cold and hot fusion reactions, see Fig. 1 and Table 1, which show examples obtained at GSI, where both reaction types have played an important role in the decades-long SHE program [11].

In the general context of this paper, we limit the considerations to those of isotope production. We neglect aspects like the energy loss/straggling and scattering of an evaporation residue (EVR) inside the target and associated constraints like those due to finite acceptance of recoil separators that may be present behind the target, not least as target performance is as relevant in studies that accept all EVRs recoiling from the paper, independent of energy or angular distribution, including experiments performed with setups as those used in refs. [14, 15]; see also target development efforts reported in this context in ref. [16]. In many hot fusion reactions, two (sometimes even three, e.g. in [17]) neighboring isotopes can be produced simultaneously, and the total useful

energy range that projectiles can have inside the target layer is quite wide. Accordingly, layers up to about  $1.5 \text{ mg/cm}^2$  can contribute to EVR production. Typical target thicknesses used in experiments, however exceeded  $0.5 \text{ mg/cm}^2$  only in few cases, and so far never exceeded a fraction of about 60%, cf. Table 1 (except for experiments without recoil separator, see [14, 15, 18]). It thus appears worth inspecting if thicker actinide targets might indeed lead to larger rates of detected superheavy nuclei (SHN).

## The optimum actinide target for SHE production

Ideally, a most intense beam would irradiate a self-supporting, elementally pure, monoisotopic, ideally-thick target. Real targets, however, deviate from this; a current overview on target production at GSI and at Johannes

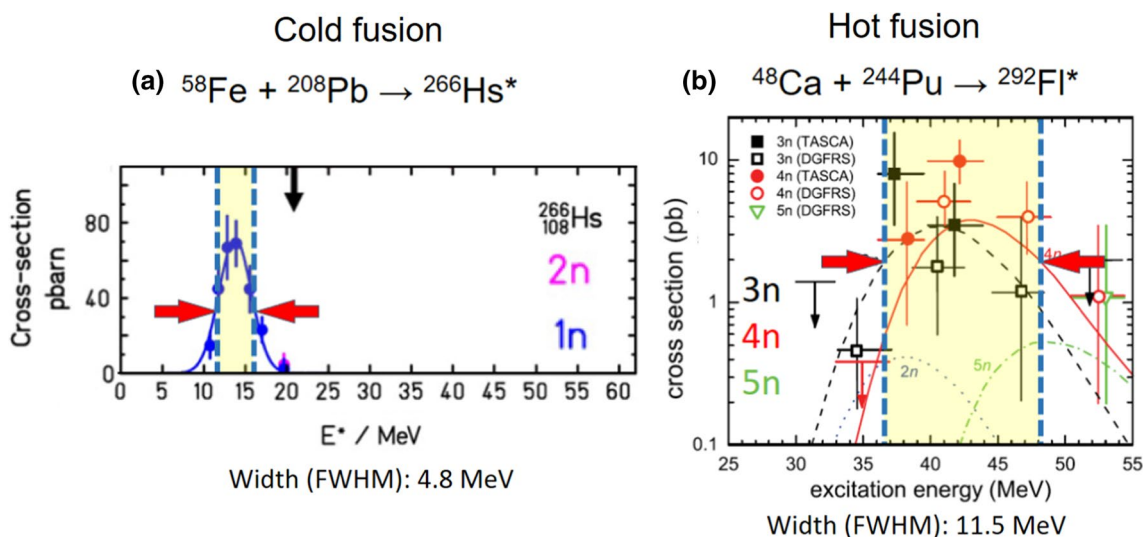


**Fig. 1** Typical excitation functions leading to superheavy elements for a  $^{208}\text{Pb}$ -target based cold fusion reaction (left panel) [12] and an actinide-target based hot fusion reaction (right panel) [13]. (Left panel reprinted and adapted from S. Hofmann, *Study of SHE at the GSI-SHIP*, Prog. Part. Nucl. Phys. 62 (2009) 337, <http://dx.doi.org/>

[10.1016/j.ppnp.2008.12.008](https://doi.org/10.1016/j.ppnp.2008.12.008). Copyright 2009, with permission from Elsevier. Right panel: Reprinted figure with permission from J. Gates et al., Phys. Rev. C 83, 054,618, 2011, <http://dx.doi.org/10.1103/PhysRevC.83.054618>. Copyright 2011 by the American Physical Society

**Table 1** Relevant parameters connected to the width of the excitation functions shown in Fig. 1

	Cold fusion reaction ( $^{58}\text{Fe} + ^{208}\text{Pb}$ )	Hot fusion reaction ( $^{48}\text{Ca} + ^{244}\text{Pu}$ )
Significant exit channel(s) accessible at a single beam energy	1n ( $^{265}\text{Hs}$ )	3n + 4n ( $^{288,289}\text{Fl}$ )
Width (FWHM) of excitation function for the above channels (MeV $E^*$ )	4.8	11.5
$E_{\text{Lab}}$ range inside target layer (MeV)	5.7	13.8
Ideal target thickness covering FWHM of excitation function ( $\text{mg/cm}^2$ )	0.45 ( $^{208}\text{Pb}$ as PbS)	1.5 ( $^{244}\text{Pu}$ as $\text{PuO}_2$ )
Typical thickness used in experiments ( $\text{mg/cm}^2$ )	0.5 (SHIP)	$\leq 0.84$ (DGFRS, TASCAs, GBS, GARIS)
Fraction of ideal thickness (%)	$\approx 110$	$\leq 55$

Gutenberg University Mainz (JGU) can be found in [19]. Only few elements can be used as targets in the form of self-supporting films. Actinide targets are always deposited on backing foils, which (i) act as additional target element leading to unwanted nuclear reaction products, (ii) cause beam particles to lose a fraction of their kinetic energy, which is converted to heat that heats the target, which may limit its experiment lifetime, and (iii) lead to an energy straggling of the projectiles, leading to a smeared-out energy distribution of projectiles entering the target, which may ultimately shift the energy range covered inside the target material to partially fall outside of the useful energy window of the excitation function. This still leads to the full heating load, but to reduced yield of the desired EVRs compared to the ideal case where all projectiles cover the optimum region of the excitation function. Additional adverse factors concern the chemical composition of the target, because actinides are never deposited in elemental, but in molecular form. Additional elements—from the target compound as well as from unwanted impurities—present in the layer will again lead to unwanted background. Finally, the finite thickness will negatively affect the experimentally reachable yield when compared to the idealized situation. On the way to improved targets, not only the aspect of higher yield has to be considered, but also the experiment lifetime of the target and the production of unwanted byproducts.

## Will thicker targets really lead to higher rates of superheavy nuclei?

The energy straggling of the beam inside the backing, or a limited acceptance of recoil separators used to isolate EVRs from beam and unwanted nuclear reaction products might prevent reaching higher production rates when going beyond current target thicknesses. Key properties of separators that were in operation 15 years ago are summarized in [20]; since then, several new and improved devices were constructed, e.g. [21–24], with many featuring larger acceptance. SHE experiments where other methods for nuclide isolation are employed, e.g., chemical separations [25, 26] without using the concept of physical preseparation [27] are not affected by the latter constraint. To our knowledge, only two experiments on heaviest elements produced in actinide-target based reactions have been performed with targets of different thickness at the same separator. The relevant aspects are displayed in Fig. 2.

The isotopes  $^{288,289}\text{Fl}$  have been produced in the  $^{48}\text{Ca} + ^{244}\text{Pu}$  reaction at TASCA. A first experiment using  $0.44\text{ mg/cm}^2$ -thick  $^{244}\text{Pu}$  targets (in the form of  $0.50\text{ mg/cm}^2\text{ PuO}_2$ ) was carried out in 2009 [13, 28] and the second one using  $0.79\text{ mg/cm}^2$ -thick targets in two runs in 2019 and 2020 [29, 33]. This latter thickness is about the maximum that can reliably be produced with the current technique [34]. The used setups differed, not least in terms of the size of the used focal plane detector ( $144 \times 48\text{ cm}^2$  [13] vs.  $60 \times 60\text{ cm}^2$  [29]) and in quadrupole magnet focusing,

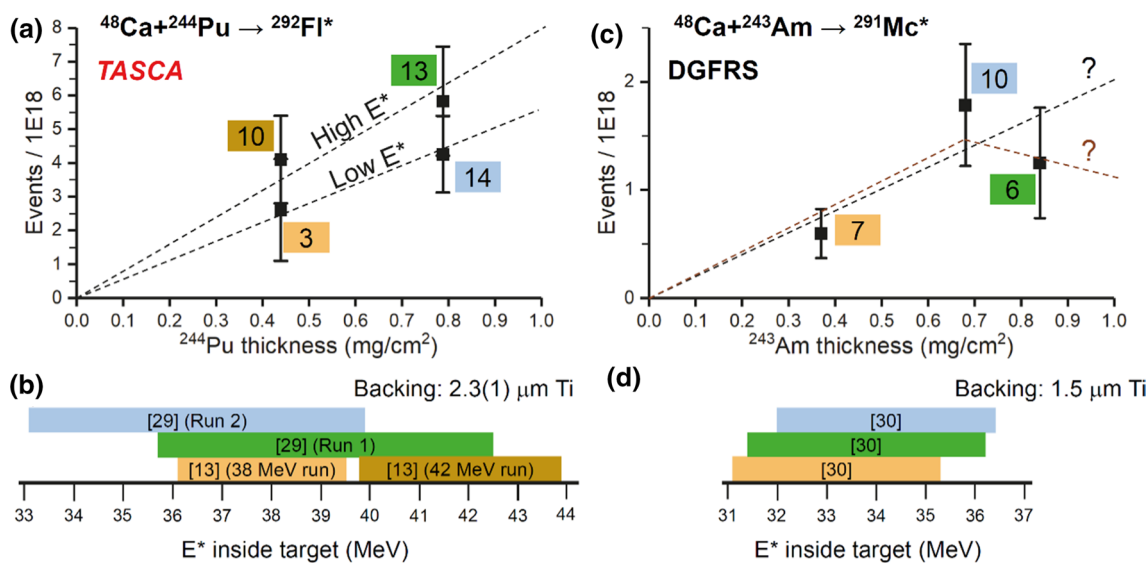


**Fig. 2** **a** Beam-dose normalized rate of detected evaporation residues for the  $^{48}\text{Ca} + ^{244}\text{Pu}$  reaction studied at TASCA [13, 28, 29]; the sum of  $3n(^{289}\text{Fl})$  and  $4n(^{288}\text{Fl})$  evaporation residues is shown; the number of detected decay chains is indicated for all data points. The dashed lines guide the eye; **b** excitation energy range covered inside the targets in the different runs. **c** Same as (a) but for the reac-

tion  $^{48}\text{Ca} + ^{243}\text{Am}$  reaction studied at the DGFRS [30, 31]; the sums of all events assigned in the original papers to the  $3n(^{288}\text{Mc})$  and  $2n(^{289}\text{Mc})$  channels are given; the question concerning the correct assignment [32] is irrelevant in the present context; **d** Same as (b) but for the different runs of the reaction displayed in panel (c)

which led to estimated efficiencies to register produced  $^{288,289}\text{Fl}$  of about 60% [13] and 30% [29, 33]. (For the first experiment, only the decay chains published in [28] are considered here.) Fig. 2a) shows that within the substantial error bars, which are dominated by statistical effects associated with small numbers of detected events, the thicker target led to roughly linearly increasing yield. Despite the smaller nominal efficiency, the normalized event rate increased. The excitation energy range covered inside the targets is shown in panel b). All four data points are compatible with increasing rate as a function of increasing target thickness. At each thickness, the data point corresponding to the higher excitation energy is higher. While the small statistics limit definite conclusions, the currently available data support that the maximum useful target thickness at TASCAs has not yet been reached.

The situation is similar in the production of Mc (element 115) isotopes in the  $^{48}\text{Ca} + ^{243}\text{Am}$  reaction at the Dubna Gas-Filled Recoil Separator (DGFRS), see Fig. 2c, d, albeit not as clear. Within uncertainties, the rate in the experiment with the thickest targets may or may not quite follow the increasing trend. Higher statistics data have recently been acquired [35] in Dubna using the DGFRS-2, which features higher acceptance than DGFRS that was used in the experiments depicted in Fig. 2.

We conclude that no clear indications exist, which suggest that the maximum useful target thickness has already been reached in the production of superheavy nuclei. Information that is more informative may be derived from simulations of EVR trajectories in gas-filled separators, which take into account all relevant effects and can predict image sizes and EVR rates in the focal plane. One such code, developed by Gregorich [36], was applied to experiments at the Berkeley Gas-filled Separator (BGS) at Lawrence Berkeley National Laboratory, Berkeley, CA, and at TASCAs, however the effects of varying target thickness have not been explicitly covered in [36]. This was done by Semchenkov [37] for the  $^{48}\text{Ca} + ^{238}\text{U}$  reaction at TASCAs. Calculated rates as function of target thickness exhibit a weakly pronounced maximum at  $\approx 0.6 \text{ mg/cm}^2$  and drop slightly towards  $1 \text{ mg/cm}^2$ , which is the highest considered thickness. As no error bars are given, the significance of this cannot be judged. Similar simulations, on the new DGFRS-2, have been published recently [38]; these consider the detected rate of EVRs from the  $^{244}\text{Pu}(^{48}\text{Ca}, 4n)$  reaction for target thicknesses up to  $0.8 \text{ mg/cm}^2$ ; according to [38], the rates are increasing steadily up to this value; the evolution of the rate vs. target thickness makes it at least questionable if  $0.8 \text{ mg/cm}^2$  would indeed be the maximum useful target thickness. Given the complex processes governing EVR trajectories in dilute gases, which are described in detail in [36], benchmarking of these codes at high target thicknesses appears important.

## Production of actinide targets—the state of the art

In the past years, almost all actinide targets for SHE production have been prepared by the molecular plating (MP) technique. This was invented in the 1960s [39] and produces layers of the actinide of choice by electrodeposition from alcoholic solution, into which the dissolved actinide starting material—often the nitrate—is initially transferred [40]. Descriptions of the setup and procedure currently used in the JGU's target lab in Mainz can be found in [34, 41]. Layers up to about  $\approx 0.8 \text{ mg/cm}^2$  thickness can be produced in a single deposition step with yields often exceeding 90%. Layer formation occurs on the cathode, which is the target backing. Typically, thin Ti foils are used nowadays for this purpose. Whereas the method has been used successfully for many decades, detailed knowledge of all relevant microscopic processes occurring during MP is still lacking; the exact nature, e.g., chemical composition of the produced films is still being explored [42] and the method is still being refined, e.g., by studying the influence of varying solvent [43]. On the way to improved targets, it therefore appears mandatory to elucidate to a fuller extent the processes underlying MP. Its further improvement towards yet more mechanically stable and thicker targets that withstand higher beam intensities over longer time periods is of high relevance in the field of superheavy element research, given the strong efforts to improve experimental capabilities by the installation of new and more powerful accelerators. The advancement of the associated target technology should go hand in hand with efforts to make improved beams available.

## Beam-induced transformations

The irradiation of freshly produced MP targets leads to transformations in the layers already at small applied beam doses. As a practical effect, the fresh layers, which are sometimes not stable over extended periods, transform into long-term stable layers. Correspondingly, the so-called “baking-in” of fresh targets, i.e., the irradiation with initially very small and step-wise increasing beam intensities over periods of only few hours has become standard. Its effects are directly noticeable, e.g., when  $\alpha$ -decaying target isotopes like  $^{248}\text{Cm}$  are used. Whereas the  $\alpha$  spectrum of a freshly produced target shows substantially broadened peaks—indicative of comparatively thick layers—these peak widths decrease immediately upon the baking-in, cf. Figure 3 in [44] and Fig. 6 in [45], indicating a loss of material during the procedure. Radioactivity measurements confirm that only non-radioactive material is lost. The effect cannot be reproduced by simple thermal treatment [46, 47]. To decouple the target baking-in from the availability of suitable Coulomb-barrier heavy-ion beams, an off-line pilot setup, the Offline Deposit Irradiator (ODIn) [48] has been



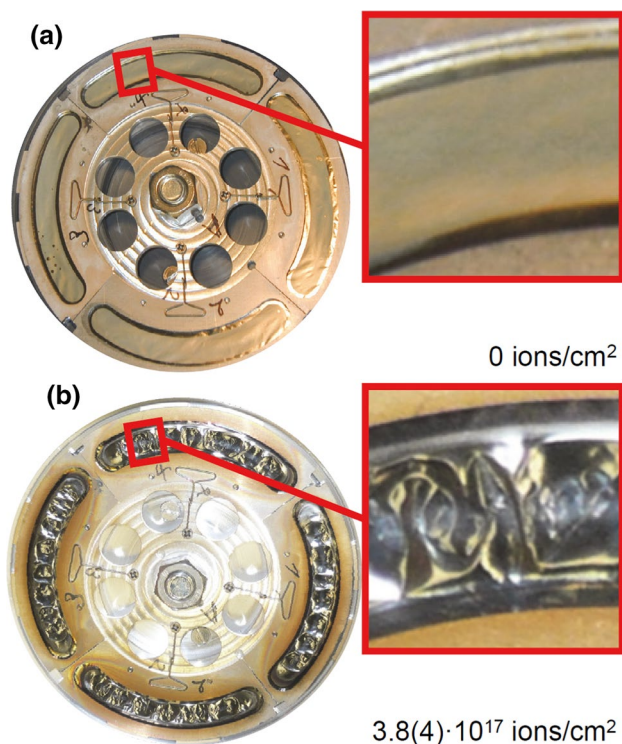


**Fig. 3** TASCA target wheel containing  $\approx 0.5\text{-mg/cm}^2$  thick  $^{249}\text{Cf}$  targets deposited on  $\approx 2.2\text{-}\mu\text{m}$  thick Ti backings. **a** freshly produced target wheel; **b** target wheel after irradiation with  $9.2(9)\cdot 10^{18}$  6.1-MeV/u  $^{50}\text{Ti}$  projectiles [53]. **b** Used with permission of Springer Nature, from E. Jäger et al., High intensity target wheel at TASCA: target wheel control system and target monitoring, *J. Radioanal. Nucl. Chem* 299 (2014) 1073, <http://dx.doi.org/10.1007/s10967-013-2645-1>. Copyright 2014, not covered under the open access license; permission conveyed through Copyright Clearance Center, Inc

constructed at Mainz University and first tests using Pb targets have been performed [49]. If successful, this may also be beneficial to induce similar changes in actinide samples that are used for off-line applications in a variety of research fields, e.g., as recoil ion sources [50, 51].

Extended irradiation with intense heavy-ion beams leads to substantially more dramatic changes [52] in actinide targets. The photographs in Fig. 3 show a TASCA target wheel [53] containing about 12.4 mg of  $^{249}\text{Cf}$ , forming a set of four  $\approx 0.5\text{ mg/cm}^2$ -thick target segments prepared from recycled material. Panel a) shows the fresh target wheel after production by MP, and panel b) shows the same target wheel after it was used in the search for element 120 in the  $^{50}\text{Ti} + ^{249}\text{Cf}$  reaction [54] in the course of a  $\approx 1$  month long search experiment, where beam intensities of  $\approx 3\text{--}6\cdot 10^{12}\text{ s}^{-1}$  ( $\approx 0.5\text{--}1.0\ \mu\text{A}_{\text{part}}$ ) were applied, delivered as a pulsed beam with 25% duty cycle (5 ms beam on/15 ms beam off). This corresponds to a four times higher intensity (i.e.,  $\approx 2\text{--}4\ \mu\text{A}_{\text{part}}$ ) during the pulse. A total beam dose of  $9.2(9)\cdot 10^{18}$   $^{48}\text{Ca}$  ions, corresponding to a fluence of  $3.8(4)\cdot 10^{17}$  ions/cm $^2$ , was applied.

Obviously, the irradiated target looks completely different; the magnified inset shows a change in color from green to black. In addition, the initially smooth foil has become wrinkled. During the experiment, a finite target segment is subjected to substantial thermal stress by being exposed to the intense heavy-ion beam for a  $< 1$  ms-long time interval every 80 ms. The target wheel rotates in a  $\approx 1$  mbar He atmosphere, which provides efficient target cooling [52]. Among the necessary tasks towards the production of targets that are thicker and that can at the same time resist higher beam currents for longer time periods, the elucidation of the transformations induced by the intense irradiation appears mandatory. Theoretical work, e.g., [52, 55] goes hand in hand with experimental studies.

### Target analytics

Several analytical studies on beam-induced effects have been described in the literature, e.g., [44, 47, 56]. Most focused on microscopic methods, and only few spectroscopic studies are reported [57]. We have set up an analytical program to understand better what a thin layer experiences by analyzing its structure before irradiation, i.e., freshly after production, as well as after irradiation. For this, we use the methods summarized in Table 2. Some are applicable to radioactive samples, whereas others only for non-active ones. With respect to f-elements, these are thus restricted to studies of lanthanide layers that are either fresh or that have been irradiated only with comparatively small fluences and afterwards allowed to sit in storage for decay of beam-induced radionuclides. Our goal is to make use of complementary methods, including spectroscopic and ion-beam-based ones. Some first results, on Pb thin films, are described in [48, 49], and further results will be published in the near future.

The analytical methods listed in Table 2 are grouped into individual families for the sake of clarity. Radiometric methods provide information on the quantities of individual isotopes, either directly if the isotope under study is sufficiently radioactive, or after activation by neutrons in the research reactor TRIGA Mainz [58]. However, many light elements (H,C,F,O) cannot easily be detected by these method, precluding a complete characterization of potentially co-deposited (organic) material. In case of  $\alpha$ -active target isotopes, some information can be obtained by the analysis of  $\alpha$  spectra [44, 45]. RI (for explanation of the abbreviations, we refer to Table 2) provides relative information on the spatial distribution of radioactive material [59–61]. Microscopic methods, e.g., true-color images in combination with high-resolution photos, give insight into changes of the film morphology due to irradiation [48, 49]. 3D laser scanning microscopy is in principle available and marks the transition to AFM in terms of spatial resolution and the possibility to

**Table 2** Analytical methods employed by us so far for the analytics of lanthanide and actinide thin films

	Abbreviation	Availability for inactive samples	Availability for radioactive samples
<i>Radiometric methods</i>			
$\alpha$ - $\gamma$ -spectrometry	$\alpha$ - $\gamma$ -spec	–	JGU
Neutron activation analysis	NAA	JGU	JGU
Radiographic imaging	RI	–	JGU
<i>Microscopic methods</i>			
Digital 3D scanning light microscope	Mic	GSI	–
Atomic force microscopy	AFM	JGU	JGU
Scanning electron microscopy	SEM	GSI, DECHEMA	JGU
<i>Spectroscopic methods</i>			
Energy dispersive X-ray spectroscopy	EDX	GSI, DECHEMA	JGU
Confocal Raman microscopy	Raman	GSI, DECHEMA	JRC
Fourier-transform infrared spectroscopy	FTIR	JGU	JRC
Nuclear magnetic resonance	NMR	MPIP	–
X-ray photoelectron spectroscopy	XPS	JRC	–
<i>Particle-induced methods/Ion-beam analysis</i>			
Elastic recoil detection analysis	ERDA	HZDR	JYFL
Rutherford backscattering spectrometry	RBS	HZDR	JYFL
Particle-induced X-ray emission	PIXE	HZDR	JYFL
<i>Diffraction-based methods</i>			
X-ray diffraction	XRD	GSI, TU DA	JRC
Grazing incidence X-ray diffraction	GIXD	KIT, TU DA	–

The third and the fourth columns indicate the institutions providing these methods in a purely non-radioactive environment and also for radioactive samples (actinide targets, activated and/or irradiated lanthanide targets), respectively

*DECHEMA* DECHEMA-Forschungsinstitut, Frankfurt, Germany, *GSI* GSI Helmholtzzentrum für Schwerionenforschung, Darmstadt, Germany, *HZDR* Helmholtz-Zentrum Dresden-Rossendorf, Germany, *JGU* Johannes Gutenberg University Mainz, Germany, *JRC* European Commission Joint Research Center (JRC), Karlsruhe, Germany, *JYFL* University of Jyväskylä, Finland, *KIT* Karlsruher Institut für Technologie, Karlsruhe, Germany, *MPIP* Max-Planck-Institut für Polymerforschung, Mainz, Germany, *TU DA* Technische Universität Darmstadt, Germany

measure, e.g., roughness parameters, but is much faster, at the cost of limited spatial resolution ( $\leq 10$  nm). State-of-the-art devices allow measurements of complete targets and determination of the total volume, yielding information on the layer density. More studies, however, were performed with AFM [42, 56, 62]. The spatial resolution of scanning probe microscopy is only limited by the size of the used tip and typically only rather small areas are scanned, which renders the method slow and difficult when information on the morphology of MP thin films is needed. For surface inspection, SEM is very common [42, 47, 62, 63], often in combination with EDX providing spatially resolved (sub- $\mu$ m range) elemental composition. Limitations arise due to the influence of the backing and the low sensitivity for light elements. Vibrational spectroscopic methods (Raman and IR spectroscopy) provide information about the chemical structure, phase and crystallinity and make ion-beam induced changes visible [64]. Identification of specific absorption bands requires published reference spectra, which are scarce

or completely missing, especially for elements beyond Pu. Confocal Raman microscopy has already proven successful in the characterization of lead targets [48, 49] and has been adapted for studies of actinides [65]. The microscopic variants of conventional vibrational spectroscopy circumvent the problems due to the challenging sample morphology. NMR spectroscopy of f-element thin films is rather difficult as many target nuclei are paramagnetic, but allows characterizing precursors used in modern approaches to the target preparation as they are currently under development [66] via the chemical shift of light nuclei in the ligand systems ( $^1\text{H}$ ,  $^{13}\text{C}$ ,  $^{19}\text{F}$ ). XPS has been rather widely adopted, especially for MP films [42, 63, 67], providing information about the elemental composition in the top surface layers of a sample and also hints at the speciation via the chemical shifts of individual elemental peaks. However, due to the challenging morphology of target films and the influence of the backings, a clear interpretation of the data is difficult. IBA methods provide insight into the elemental composition (ERDA,

RBS) and elemental distribution (PIXE) of thin films [57], but are also limited with respect to light elements (H,C,F,O). Diffraction-based methods are in principle preferred as reference data are available, also for post-plutonium actinides. However, previous attempts using such methods failed due to the amorphous nature of the thin films [63], and problems due to the rather thick and rough backing [47].

## On the way to the optimum target—and backing

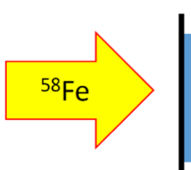
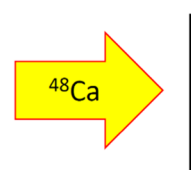
Besides the layer of the f-element, also the substrate on which it is deposited has to be considered. As will be shown below, the backing contributes to a dominating extent to the target heating in beam, as follows from energy-loss considerations summarized in Fig. 4.

The beam-induced target heating may be sufficient to heat the target to the point of mechanical failure. Figure 4 shows that cold fusion reactions with lead targets make use of very thin backings (tens of  $\mu\text{g}/\text{cm}^2$  of carbon) [69], onto which the target material (typically  $0.3\text{--}0.5\text{ mg}/\text{cm}^2$ ) is evaporated in the form of chemical compounds with high melting points [70] like PbS. The total energy loss inside the backing and the target layer is about 6.9 MeV, which corresponds to a heating power of 6.9 W per  $6.24 \cdot 10^{12}$  projectiles/s. In the case of actinide-based reactions, this is different, because electroplating onto such thin and fragile carbon foils is difficult. While it has been demonstrated for relatively small circular targets [71], depositions on extended banana-shaped segments as they are used in rotating target wheels (cf. Figure 3) have not been produced to date. Most labs therefore use few- $\mu\text{m}$  thin titanium backings, which are sufficiently mechanically stable and can be produced in pinhole-free quality by cold rolling [72]. The energy loss of a  $^{48}\text{Ca}$  beam of appropriate energy inside a 2.2- $\mu\text{m}$  Ti backing is

13.4 MeV, a factor of 11 higher than in the C backing used for cold fusion reactions! The energy loss inside the target layer, which is thicker and comprises a heavier target element, is also slightly higher than in the case of the cold fusion reaction. Overall, the beam-induced heating is about 3 times higher and may well be a limiting factor of the useful lifetime of an actinide target. As the backing contributes the major part and is not necessarily fixed to Ti from the point of view of the experiment, it is worthwhile to consider alternative backing materials. One constraint will be to avoid the production of  $\alpha$ -decaying isotopes in the interaction of the beam with the target material, as these would contribute to unwanted background in the  $\alpha$ -spectra that are typically recorded to identify single superheavy nuclei. The sum of the atomic numbers of the beam and of the target must therefore stay below 75. In case of a  $^{48}\text{Ca}$  beam, elements with  $Z < 55$  can therefore be considered. The list of elements from which thin mechanically stable foils can be made is comparatively short and includes the 7 elements which are listed in Table 3 along with the minimum thickness in which mechanically suitable foils of these elements are available. The energy loss of a 250-MeV  $^{48}\text{Ca}$  beam in such a foil is given, and for completeness also the melting point, which should be high, and the thermal expansion coefficient, which ideally is small.

Table 3 reveals that Al, which was also tried [72], may not be a very good choice because the melting point is smaller and the thermal expansion coefficient is much larger than for Ti. However, C is standing out because it can be produced into very thin foils and features by far the smallest energy loss, a very high melting point, and also a thermal expansion coefficient that is smaller than that of Ti. Therefore, efforts along the lines described in [71] may be worthwhile pursuing to produce actinide targets with improved performance. Even if very thin backings like they are useable for targets produced by thermal evaporation or by sputtering may not

**Fig. 4** Contributions to the total energy loss dE per beam ion in typical cold fusion and hot fusion reactions carried out at GSI. Due to the pulsed beam, this is applied inhomogeneously. The energy loss is calculated with the SRIM program package [68]. Note that experiments in Dubna typically use 1.5  $\mu\text{m}$  Ti backing instead of 2.2  $\mu\text{m}$  ones; this reduces the energy-loss in the backing by 4.2 MeV and hence the average heating power to 16.5 W/ $\mu\text{A}_{\text{part}}$ . ( $1\ \mu\text{A}_{\text{part}} = 6.24 \cdot 10^{12}$  projectiles/s)

	Cold fusion			Hot fusion		
	$^{58}\text{Fe} + ^{208}\text{Pb} \rightarrow ^{266}\text{Hs}^*$			$^{48}\text{Ca} + ^{244}\text{Pu} \rightarrow ^{292}\text{Fl}^*$		
						
	dE			dE		
Backing	40 $\mu\text{g}/\text{cm}^2$	C	1.2 MeV	2.2 $\mu\text{m}$	Ti	13.4 MeV
Target	0.45 $\text{mg}/\text{cm}^2$ (0.38 $\text{mg}/\text{cm}^2$ $^{208}\text{Pb}$ )	PbS	5.7 MeV	0.90 $\text{mg}/\text{cm}^2$ (0.80 $\text{mg}/\text{cm}^2$ $^{244}\text{Pu}$ )	$\text{PuO}_2$	7.3 MeV
Total	6.9 MeV			20.7 MeV		
Heating	6.9 W/ $\mu\text{A}_{\text{part}}$			20.7 W/ $\mu\text{A}_{\text{part}}$		

**Table 3** Selected properties of potentially suitable backing materials

Element	dE/dX <sup>a</sup> (MeV / mg cm <sup>2</sup> )	Typical thickness	dE <sup>b</sup> (MeV)	m <sub>p</sub> (°C)	Thermal expansion coefficient (μm / m K)
<sup>4</sup> Be	17.4	10 μm	32.1	1278	11.3
<sup>6</sup> C	19.0	40–200 μg/cm <sup>2</sup> (0.18–0.89 μm)	0.8–3.8	3500	7.1
<sup>13</sup> Al	15.9	1 μm	8.6	660	23.1
<sup>22</sup> Ti	13.7	1.5 <sup>c</sup> –2.2 <sup>d</sup> μm	9.3–13.6	1660	8.6
<sup>28</sup> Ni	12.7	1 μm	11.3	1453	13.4
<sup>40</sup> Zr	10.4	1 μm	6.8	1852	5.7
<sup>46</sup> Pd	9.8	1 μm	11.8	1552	11.8

<sup>a</sup>For 250 MeV <sup>48</sup>Ca beam [68]

<sup>b</sup>For 250 MeV <sup>48</sup>Ca beam inside a layer of the given typical thickness

<sup>c</sup>Typical value used in Dubna

<sup>d</sup>Typical value used at TASCA

ultimately be achievable, carbon may still be the best backing material. When used in gas-filled separators, sources of O<sub>2</sub> like impurities in the filling gas or the deposition of the target element in oxidic form need to be considered, as a hot C layer may act as an oxygen getter, transforming into gaseous CO/CO<sub>2</sub>.

## Conclusion

We summarized some key aspects that are relevant on the way towards the production of targets with improved beam tolerance, as they will be needed to accommodate the ever-increasing beam intensities of new accelerator facilities that come online in the superheavy element laboratories. Our overall goal is the development of target production methods that yield actinide films, which are sufficiently thick, do not contain problem contaminants, adhere to the optimum backing, are beam resistant, and can be reprocessed. Our approach so far has been to analyze the molecular plating process as a first step. A second step will be to understand better what happens to molecular plated layers in the beam, and as a third step to improve molecular plating for thick targets or develop better methods. Finally, attention should be paid to the choice of the backing material.

**Acknowledgements** We appreciate the continued support of the mechanical workshop and the reactor operation staff at the Research Reactor TRIGA Mainz. We acknowledge Elif Celik Ayik, Annett Hübner, Jutta Steiner und Vera Yakusheva of the GSI Target laboratory, discussions with Jadamba Khuyagbaatar in the GSI SHE-Chemistry department, as well as support in the ongoing thin layer production and characterizations by Beatriz Sánchez Batalla and Jürgen Schuster (DEHEMA Frankfurt), Markus Bender, Ioannis Tzifas, Alexey Prosvetov, Pascal Simon and Marilena Tomut (GSI Darmstadt), Primiana Cavallo, Tobias Häger, Evgenia Schaffner (JGU Mainz), Olaf Walter, Jean-Yves Colle and Thomas Gouder (JRC Karlsruhe), Joachim Brötz

and Marton Major (TU Darmstadt), Jaakko Julin, Mikko Laitinen and Timo Sajavaara (Univ. Jyväskylä) and Peter Weidler (KIT). This project received funding from the German BMBF (project 05P21UMFN2). Access to the ActUsLab/PAMEC and ActUsLab/FMR facilities was granted under the Framework of access to the Joint Research Centre Physical Research Infrastructures of the European Commission (Projects Targets-SHE1, Research Infrastructure Access Agreement N° 36106/01 and Targets-SHE2, Research Infrastructure Access Agreement N° 36107/01). Any opinions, findings and conclusions or recommendations expressed in this paper are those of the authors and do not necessarily reflect those of the European Commission.

**Funding** Open Access funding enabled and organized by Projekt DEAL.

## Declarations

**Conflict of interest** The authors declare no competing interest.

**Open Access** This article is licensed under a Creative Commons Attribution 4.0 International License, which permits use, sharing, adaptation, distribution and reproduction in any medium or format, as long as you give appropriate credit to the original author(s) and the source, provide a link to the Creative Commons licence, and indicate if changes were made. The images or other third party material in this article are included in the article's Creative Commons licence, unless indicated otherwise in a credit line to the material. If material is not included in the article's Creative Commons licence and your intended use is not permitted by statutory regulation or exceeds the permitted use, you will need to obtain permission directly from the copyright holder. To view a copy of this licence, visit <http://creativecommons.org/licenses/by/4.0/>.

## References

- Oganessian YT, Utyonkov VK (2015) Super-heavy element research. Rep Prog Phys 78:036301
- Düllmann CE, Herzberg R-D, Nazarewicz W, et al (eds) (2015) Special issue on superheavy elements. Nucl Phys A 944
- Münzenberg G (2015) From bohrium to copernicium and beyond SHE research at SHIP. Nucl Phys A 944:5–29



4. Morita K (2015) SHE research at RIKEN/GARIS. *Nucl Phys A* 944:30–61
5. Stodel C, Libin J-F, Marry C et al (2015) High intensity targets stations for S3. *J Radioanal Nucl Chem* 305:761–767
6. Dmitriev SN, Popeko AG (2015) High-power radioactive targets as one of the key problems in further development of the research program on synthesis of new superheavy elements. *J Radioanal Nucl Chem* 305:927–933
7. Haba H (2019) A new period in superheavy-element hunting. *Nat Chem* 11:10–13
8. Miski-Oglu M, Aulenbacher K, Barth W, et al (2019) Progress in SRF CH-cavities for the HELIAC cw linac at GSI. In: 19th international conference on RF Superconductivity, JACoW Publishing, Dresden, Germany
9. Dmitriev S, Itkis M, Oganessian Y (2016) Status and perspectives of the Dubna superheavy element factory. *EPJ Web Conf* 131:08001
10. Drouart A, Amthor AM, Boutin D et al (2010) The super separator spectrometer (S3) for SPIRAL2 stable beams. *Nucl Phys A* 834:747c–750c
11. Düllmann CE, Block M, Heßberger FP et al (2022) Five decades of GSI superheavy element discoveries and chemical investigation. *Radiochim Acta* 110:417–439
12. Hofmann S, Ackermann D, Antalic S et al (2007) Studies of superheavy elements at SHIP. *Int J Modern Phys E* 16:937–947
13. Gates JM, Düllmann CE, Schädel M et al (2011) First superheavy element experiments at the GSI recoil separator TASCA: the production and decay of element 114 in the  $^{244}\text{Pu}(^{48}\text{Ca},3-4n)$  reaction. *Phys Rev C* 83:054618
14. Eichler R, Aksenov NV, Belozero AV et al (2007) Chemical characterization of element 112. *Nature* 447:72–75
15. Eichler R, Aksenov NV, Albin YV et al (2010) Indication for a volatile element 114. *Radiochim Acta* 98:133–139
16. Usoltsev I, Eichler R, Vostokin GK et al (2013) Preparation and high intensity heavy ion irradiation tests of intermetallic  $^{243}\text{Am}/\text{Pd}$  targets. *Nucl Instrum Meth B* 318:297–305
17. Dvorak J, Brüchle W, Chelnokov M et al (2008) Observation of the 3n evaporation channel in the complete hot-fusion reaction  $^{26}\text{Mg}+^{248}\text{Cm}$  leading to the new superheavy nuclide  $^{271}\text{Hs}$ . *Phys Rev Lett* 100:132503
18. Stoyer NJ, Landrum JH, Wilk PA et al (2007) Chemical identification of a long-lived isotope of dubnium, a descendant of element 115. *Nucl Phys A* 787:388c–395c
19. Lommel B, Düllmann CE, Kindler B, et al Status and developments of target production for research on heavy and superheavy nuclei and elements. *Eur Phys J A* (submitted)
20. Düllmann CE (2008) Physical separators for the heaviest elements. *Nucl Instrum Meth B* 266:4123–4130
21. Popeko AG, Yeremin AV, Malyshev ON et al (2016) Separator for heavy element spectroscopy—velocity filter SHELS. *Nucl Instrum Meth B* 376:140–143
22. Oganessian YT, Utyonkov VK, Popeko AG et al (2022) DGFRS-2—a gas-filled recoil separator for the Dubna super heavy element factory. *Nucl Instrum Meth A* 1033:166640
23. Kaji D, Morimoto K, Sato N et al (2013) Gas-filled recoil ion separator GARIS-II. *Nucl Instrum Meth B* 317:311–314
24. Back BB (2017) The AGFA and AIRIS separators at ATLAS. *EPJ Web Conf* 163:00003
25. Türler A, Eichler R, Yakushev A (2015) Chemical studies of elements with  $Z \geq 104$  in gas phase. *Nucl Phys A* 944:640–689
26. Nagame Y, Kratz JV, Schädel M (2015) Chemical studies of elements with  $Z \geq 104$  in liquid phase. *Nucl Phys A* 944:614–639
27. Düllmann CE, Folden CM III, Gregorich KE et al (2005) Heavy-ion-induced production and physical pre-separation of short-lived isotopes for chemistry experiments. *Nucl Instrum Meth A* 551:528–539
28. Düllmann CE, Schädel M, Yakushev A et al (2010) Production and decay of element 114: High cross sections and the new nucleus  $^{277}\text{Hs}$ . *Phys Rev Lett* 104:252701
29. Sâmark-Roth A, Cox DM, Rudolph D et al (2021) Spectroscopy along flerovium decay chains: discovery of  $^{280}\text{Ds}$  and an excited state in  $^{282}\text{Cn}$ . *Phys Rev Lett* 126:032503
30. Oganessian YT, Abdullin FS, Dmitriev SN et al (2013) Investigation of the  $^{243}\text{Am}+^{48}\text{Ca}$  reaction products previously observed in the experiments on elements 113, 115, and 117. *Phys Rev C* 87:014302
31. Oganessian YT, Abdullin FS, Dmitriev SN et al (2012) New Insights into the  $^{243}\text{Am}+^{48}\text{Ca}$  reaction products previously observed in the experiments on elements 113, 115, and 117. *Phys Rev Lett* 108:022502
32. Forsberg U, Rudolph D, Andersson L-L et al (2016) Recoil- $\alpha$ -fission and recoil- $\alpha$ - $\alpha$ -fission events observed in the reaction  $^{48}\text{Ca} + ^{243}\text{Am}$ . *Nucl Phys A* 953:117–138
33. Sâmark-Roth A, Cox DM, Rudolph D, et al (2022) Spectroscopy along flerovium decay chains. *Phys Rev C* (submitted)
34. Runke J, Düllmann CE, Eberhardt K et al (2014) Preparation of actinide targets for the synthesis of the heaviest elements. *J Radioanal Nucl Chem* 299:1081–1084
35. Oganessian YT, Utyonkov VK, Kovrizhnykh ND et al (2022) First experiment at the super heavy element factory: high cross section of  $^{288}\text{Mc}$  in the  $^{243}\text{Am}+^{48}\text{Ca}$  reaction and identification of the new isotope  $^{264}\text{Lr}$ . *Phys Rev C* 106:L031301
36. Gregorich KE (2013) Simulation of recoil trajectories in gas-filled magnetic separators. *Nucl Instrum Meth A* 711:47–59
37. Semchenkov A (2022) Expected TASCA performance from Monte Carlo-Simulations, TASCA Commissioning Kick-Off Meeting, Presented at "TASCA Commissioning Kick-Off Meeting", GSI Darmstadt, Germany, May 15, 2006. Available at <https://indico.gsi.de/event/15605/>. (Accessed Oct. 4, 2022)
38. Solovyev DI, Kovrizhnykh ND (2022) Simulations of recoil trajectories in Dubna Gas-Filled Recoil Separator 2 by GEANT4 toolkit. *J Inst* 17:P07033
39. Parker W, Falk R (1962) Molecular plating: a method for the electrolytic formation of thin inorganic films. *Nucl Instrum Meth* 16:355–357
40. Trautmann N, Folger H (1989) Preparation of actinide targets by electrodeposition. *Nucl Instrum Meth A* 282:102–106
41. Eberhardt K, Brüchle W, Düllmann CE et al (2008) Preparation of targets for the gas-filled recoil separator TASCA by electrochemical deposition and design of the TASCA target wheel assembly. *Nucl Instrum Meth A* 590:134–140
42. Vascon A, Santi S, Isse AA et al (2012) Elucidation of constant current density molecular plating. *Nucl Instrum Meth A* 696:180–191
43. Vascon A, Santi S, Isse AA et al (2013) Smooth crack-free targets for nuclear applications produced by molecular plating. *Nucl Instrum Meth A* 714:163–175
44. Hofmann S, Heinz S, Mann R et al (2012) The reaction  $^{48}\text{Ca} + ^{248}\text{Cm} \rightarrow ^{296}116^*$  studied at the GSI-SHIP. *Eur Phys J A* 48:62
45. Brewer NT, Utyonkov VK, Rykaczewski KP et al (2018) Search for the heaviest atomic nuclei among the products from reactions of mixed-Cf with a  $^{48}\text{Ca}$  beam. *Phys Rev C* 98:024317
46. Burns JD, Myhre KG, Sims NJ et al (2016) Effects of annealing temperature on morphology and thickness of samarium electrodeposited thin films. *Nucl Instrum Meth A* 830:95–101
47. Mayorov DA, Tereshatov EE, Werke TA et al (2017) Heavy-ion beam induced effects in enriched gadolinium target films prepared by molecular plating. *Nucl Instrum Meth B* 407:256–264
48. Haas R, Meyer C-C, Böhland S et al (2020) ODI—A setup for Off-line Deposit Irradiations of thin layers for nuclear physics applications. *Nucl Instrum Meth A* 957:163366

49. Meyer C-C, Dragoun A, Düllmann CE et al (2022) Chemical conversions in lead thin films induced by heavy-ion beams at Coulomb barrier energies. *Nucl Instrum Meth A* 1028:166365
50. Götz S, Raeder S, Block M, et al (2021) Rapid extraction of short-lived isotopes from a buffer gas cell for use in gas-phase chemistry experiments. Part I: off-line studies with  $^{219}\text{Rn}$  and  $^{221}\text{Fr}$ . *Nucl Instrum Meth A* 995:165090
51. Haas R, Hufnagel M, Abrosimov R et al (2020) Alpha spectrometric characterization of thin  $^{233}\text{U}$  sources for  $^{229\text{(m)}}\text{Th}$  production. *Radiochim Acta* 108:923–941
52. Sagaidak RN (2021) Effects of beam wobbling and target rotation on the target temperature in experiments with intense heavy ion beams. *Phys Rev Accel Beams* 24:083001
53. Jäger E, Brand H, Düllmann CE et al (2014) High intensity target wheel at TASCA: target wheel control system and target monitoring. *J Radioanal Nucl Chem* 299:1073–1079
54. Düllmann CE, Yakushev A, Khuyagbaatar J, et al. Study of the  $^{50}\text{Ti} + ^{249}\text{Cf}$  fusion-evaporation reaction leading to element 120 at the gas-filled recoil separator TASCA (to be published).
55. Stodel C, Toulemonde M, Fransen C et al (2020) “Thermal Spike” model applied to thin targets irradiated with swift heavy ion beams at few MeV/u. *EPJ Web Conf* 229:05001
56. Watson PR, Loveland W, Zielinski PM et al (2004) Changes in surface composition and morphology of UF<sub>4</sub> targets during heavy ion irradiation. *Nucl Instrum Meth B* 226:543–548
57. Stodel C (2020) Methods of targets’ characterization. *EPJ Web Conf* 229:02001
58. Eberhardt K, Geppert C (2019) The research reactor TRIGA Mainz – a strong and versatile neutron source for science and education. *Radiochim Acta* 107:535–546
59. Liebe D, Eberhardt K, Hartmann W et al (2008) The application of neutron activation analysis, scanning electron microscope, and radiographic imaging for the characterization of electrochemically deposited layers of lanthanide and actinide elements. *Nucl Instrum Meth A* 590:145–150
60. Klemenčič H, Benedik L (2010) Alpha-spectrometric thin source preparation with emphasis on homogeneity. *Appl Radiat Isot* 68:1247–1251
61. Haas R, Lohse S, Düllmann CE et al (2017) Development and characterization of a Drop-on-Demand inkjet printing system for nuclear target fabrication. *Nucl Instrum Meth A* 874:43–49
62. Sadi S, Paulenova A, Watson PR et al (2011) Growth and surface morphology of uranium films during molecular plating. *Nucl Instrum Meth A* 655:80–84
63. Choi J, Chung YH (2016) Preparation of lanthanum oxide and lanthanum oxycarbonate layers on titanium by electrodeposition with organic solution. *J Nanomat* 2016:5140219
64. Tracy CL, Lang M, Zhang F et al (2015) Phase transformations in Ln<sub>2</sub>O<sub>3</sub> materials irradiated with swift heavy ions. *Phys Rev B* 92:174101
65. Naji M, Colle J-Y, Beneš O et al (2015) An original approach for Raman spectroscopy analysis of radioactive materials and its application to americium-containing samples. *J Raman Spectrosc* 46:750–756
66. Meyer C-C, Artes E, Bender M, et al (2022) Production and irradiation of lanthanide targets with high surface weights. *Radiochim. Acta* (in preparation for submission).
67. Myhre KG, Delashmitt JC, Sims NJ et al (2018) Samarium thin films molecular plated from N, N-dimethylformamide characterized by XPS. *Surf Sci Spect* 25:024003
68. Ziegler JF (2004) SRIM-2003. *Nucl Instrum Meth B* 219–220:1027–1036
69. Lommel B, Hartmann W, Kindler B et al (2002) Preparation of self-supporting carbon thin films. *Nucl Instrum Meth A* 480:199–203
70. Kindler B, Ackermann D, Hartmann W et al (2006) Chemical compound targets for SHIP on heated carbon backings. *Nucl Instrum Meth A* 561:107–111
71. Greene JP, Ahmad I (2008) Molecular plating of actinides on thin backings. *Nucl Instrum Meth A* 590:131–133
72. Lommel B, Brüchele W, Eberhardt K et al (2008) Backings and targets for chemical and nuclear studies of transactinides with TASCA. *Nucl Instrum Meth A* 590:141–144

**Publisher's Note** Springer Nature remains neutral with regard to jurisdictional claims in published maps and institutional affiliations.